Regular Article

INORGANIC CHEMISTRY RESEARCH
Published by the
Iranian Chemical Society
www.inorgchemres.org
info@inorgchemres.org

Inorg. Chem. Res., *Vol. 5, No. 2, 173-192, December 2021*
DOI: 10.22036/icr.2021.278938.1101

C–X *vs*. C–H Activation for the Ssynthesis of the Cyclometalated Complexes [Pd(YPhbpy)X] (HPhbpy = 6-Phenyl-2,2'-bipyridine; X/Y = (Pseudo)halides)

René von der Stück[a], Simon Schmitz[a] and Axel Klein[a,b,*]

[a]*Universität zu Köln, Department Für Chemie, Institut Für Anorganische Chemie, Greinstraße 6, D-50939 Köln, Germany*

[b]*Chemistry Department Faculty of Science, Shiraz University, Shiraz 71454, Iran*

(Received 30 March 2021, Accepted 25 May 2021)

The organometallic Pd(II) complexes [Pd(Phbpy)X] (X = Cl, Br, or I) containing the tridentate C^N^N cyclometalating ligand 6-(phen-2-ide)-2,2'-bipyridine (–Phbpy) were synthesised through oxidative addition using the protoligands X–Phbpy (X = Cl, Br and I) and $[Pd_2(dba)_3]$ tris(dibenzylideneacetone)dipalladium(0) in yields ranging from 23 to 51%. Further complexes [Pd(YPhbpy)Cl] resulted from C–H palladation of the protoligand derivatives Y–Phbpy with Y = F, Cl, Br, H, HO, MeO and triflate) with K_2PdCl_4 in yields ranging from 52 to 98%. All protoligands and Pd(II) complexes were fully characterised using mass spectrometry (MS), nuclear magnetic resonance (NMR) spectroscopy, and single crystal X-ray diffraction (XRD) for Y = F, MeO. The complexes were studied in detail using electrochemical (cyclic voltammetry) and spectroelectrochemical (UV-Vis absorption) methods and UV-Vis absorption spectroscopy. Relative shifts in the potentials of the ligand centred electrochemical reductions in the range –1.7 to –2.7 (*vs.* ferrocene/ferrocenium) or the Pd–X centred oxidations around +1 V are in excellent agreement with variations in the density functional theory (DFT) calculated highest occupied molecular orbitals (HOMO) and lowest unoccupied molecular orbitals (LUMO) constitutions. Long-wavelength absorption maxima attributable to metal(d)-to-ligand(π*) charge transfer transition observed in the range 350-550 nm were successfully modelled using time-dependent methods (TD-DFT) showing small contributions from triplet states.

Keywords: Palladium, Cyclometalation, C–X Activation, C–H Activation, Spectroelectrochemistry

INTRODUCTION

Cyclometalation reactions are generally of high interest in view of their role in C–H functionalisations in organometallic catalysis for the frequent case in which close-lying donor/ligand functions facilitate the so called *ortho*-functionalisation, or *directing group (DG) approach* [1-17]. At the same time cyclometalating heteroaromatic ligands such as bidentate C^N ligand 2-(phen-2-ide)-pyridine (–Phpy) [4,17-27], the tridentate C^N^N ligand 6-(phen-2-ide)-2,2'-bipyridine (–Phbpy) [28-40] or related C^N^N, N^C^N, N^C^C^N, or N^C^O^N ligands [41-46] have been used to synthesise corresponding organopalladium(II) complexes. Applications of such complexes have been reported in catalysis [4,8,17,18,21,22,25,47-50], as luminescent [23,29-31,35,36,38,41-46] or cytotoxic materials [26,28,33,51].

The first Pd(II) complex of the cyclometalating anionic –Phbpy ligand [Pd(Phbpy)Cl] was prepared in 1990 [37-40] alongside with the Pt(II) derivative [39,52-55] from K_2MCl_4 (M = Pt [39,40,54] or Pd [38-40]) or $[Pt(Me)Cl(SMe_2)_2]$ [52] and the H–Phbpy protoligand (ligand precursor, prior to deprotonation) through a cyclometalating C–H activation under relatively mild conditions for Pd(II): MeOH/ambient temperature [38], MeCN/H_2O/reflux [39] and a bit harsher for Pt(II): acetic acid/100 °C [54], Some time ago, the Ni(II) complex [Ni(Phbpy)Br] has been added to this series, but it had to be prepared by oxidative addition of the Br–Phbpy protoligand and the Ni(0) precursor $[Ni(0)(COD)_2]$ (COD = 1,5-cyclooctadiene), since the method applied for Pd and Pt

*Corresponding author. E-mail: axel.klein@uni-koeln.de

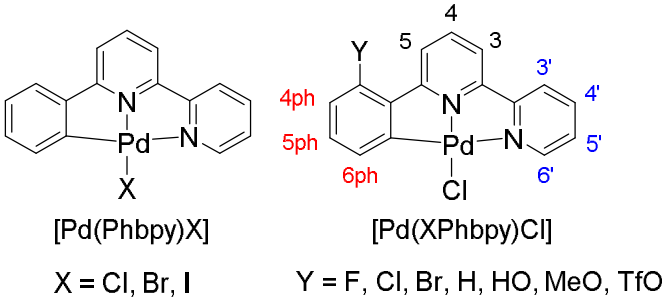

Scheme 1. Schematic of the Pd complexes with numbering

had failed [56-58]. However, very recently we succeeded in preparing the complex [Ni(Phbpy)Br] through a base-assisted C–H activation/cyclometalation [59].

These two preparation methods A) Pd(II) + H–Phbpy and B) Pd(0) + X–Phbpy represent also the typical scheme when it comes to comparison between Pd-based C–H and C–X activation/functionalisation in catalysis [60-62], while comparative studies using the same oxidation state for both types of activation remained scarce [60,61], or were based on calculations based on the density functional theory (DFT) [61-64]. Also for Ir(I) [65], Rh(I) [66] and Pt(II) [67-69], only a few comparative studies have been reported.

Herein, we report on a study dedicated to two series of cyclometalated Pd complexes [Pd(Phbpy)X] with X = Cl, Br, and I (Scheme 1) and [Pd(YPhbpy)Cl] with Y = F, Cl, Br, I, H, HO, MeO, triflate (TfO) (Scheme 1). The complexes were prepared from either oxidative addition to the C–X function of the so-called protoligands X–Phbpy or C–H activation of H–(X)Phbpy of the same protoligands and those of an extended series H–(Y)Phbpy. We compare yields, purity and preparative time and overall efforts of the two routes. Furthermore, we present for the first time comprehensive structural (single crystal X-ray diffraction-XRD) and spectroscopic (nuclear magnetic resonance (NMR), UV-Vis absorption) and (spectro)electrochemical data allowing insight into the electronic structures of these complexes and the impact of the substituents.

RESULTS AND DISCUSSION

Preparations and Analytical Characterisation

The 6-phenyl-2,2'-bipyridine protoligand (ligand prior to C–H activation and coordination) H–Phbpy was prepared through slight variation of an established procedure [59]. The protoligands (ligand prior to C–X activation and coordination) X–Phbpy/Y–Phbpy with X/Y = F, Cl, Br, I, HO, MeO and TfO were synthesised and characterised as outlined in the Supplementary Information (Figs. S1 to S14, Table S1).

The complexes [Pd(Phbpy)X] with X = Cl, Br, I were synthesised from the X–Phbpy and [$Pd_2(dba)_3$] (dba = dibenzylidineacetone) in isolated yields ranging from 23 to 51% and represent the oxidative addition C–X activation (Pathway (1) in Scheme 2). Black precipitates and the unreacted protoligands (NMR) were observed in the crude reaction mixtures. Reacting X–Phbpy (X = F, HO, MeO, TfO) and [$Pd_2(dba)_3$] did not yield the desired products.

In contrast to this, all Y–Phbpy protoligands were successfully reacted with $K_2[PdCl_4]$ yielding the complexes [Pd(YPhbpy)Cl] in yields ranging from 52 to 98% (Pathway 2 in Scheme 2). Reacting H–Phbpy under these conditions gave the parent complex [Pd(Phbpy)Cl] in 78% yield. The reported yield from a reaction in H_2O was 86% [39]. The complex [Pd(IPhbpy)Cl] was observed during synthesis but turned out to be not stable upon workup.

^{1}H NMR spectroscopy, CHN elemental analyses and electron ionisation mass spectrometry in the positive mode (EI(+)) allowed to unequivocally characterise the new complexes (full data in the Experimental Section, Figs. S15 to S17). A marked low-field shift of the 6' proton (for numbering, see Scheme 2) on the peripheral pyridine unit characterises the series [Pd(Phbpy)X] with the deshielding by the X atoms increased along the series Cl < Br < I which is paralleling their size and electronegativity (Fig. 1). The

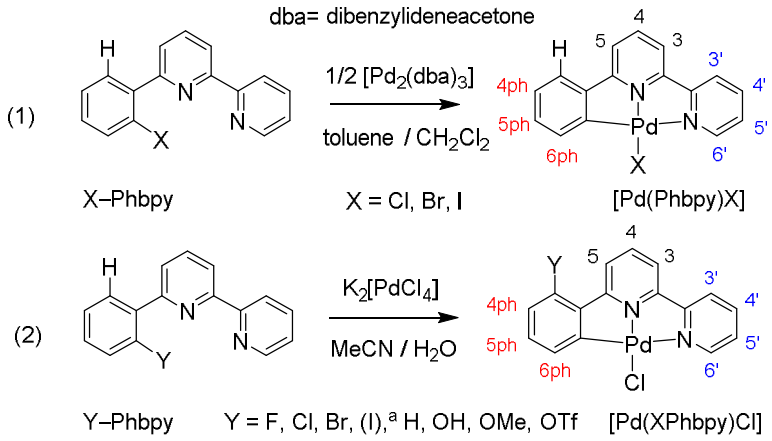

Scheme 2. Syntheses of the Pd complexes using two different methods. [a]The complex [Pd(IPhbpy)Cl] was observed during synthesis but turned out to be not stable during workup.

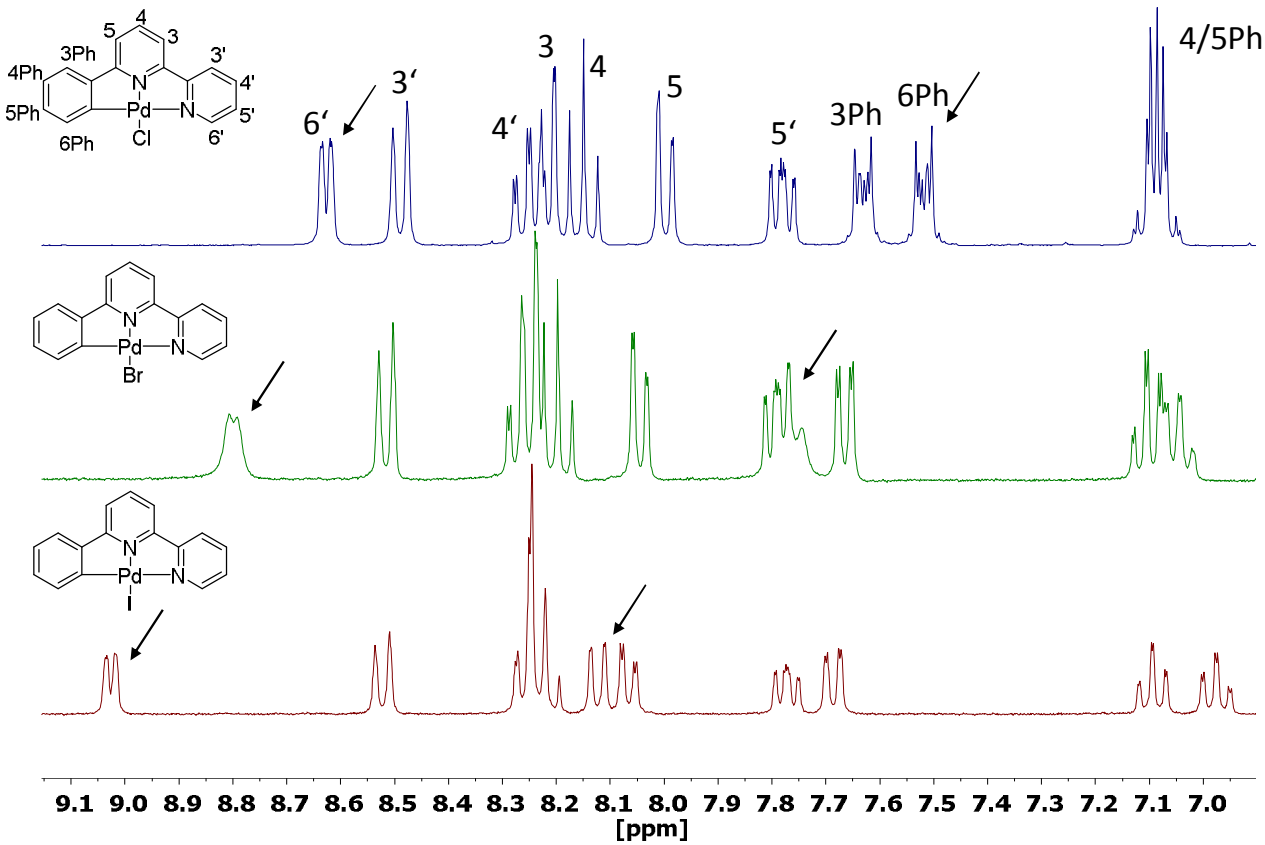

Fig. 1. 300 MHz ^{1}H NMR spectra of the complexes [Pd(Phbpy)X] (X = Cl, Br, I) in DMSO-d_6. The arrows mark the signals for the H6' proton (low field) and H6Ph (high field). Both are markedly deshielded through the interaction with the X coligand Cl < Br < I.

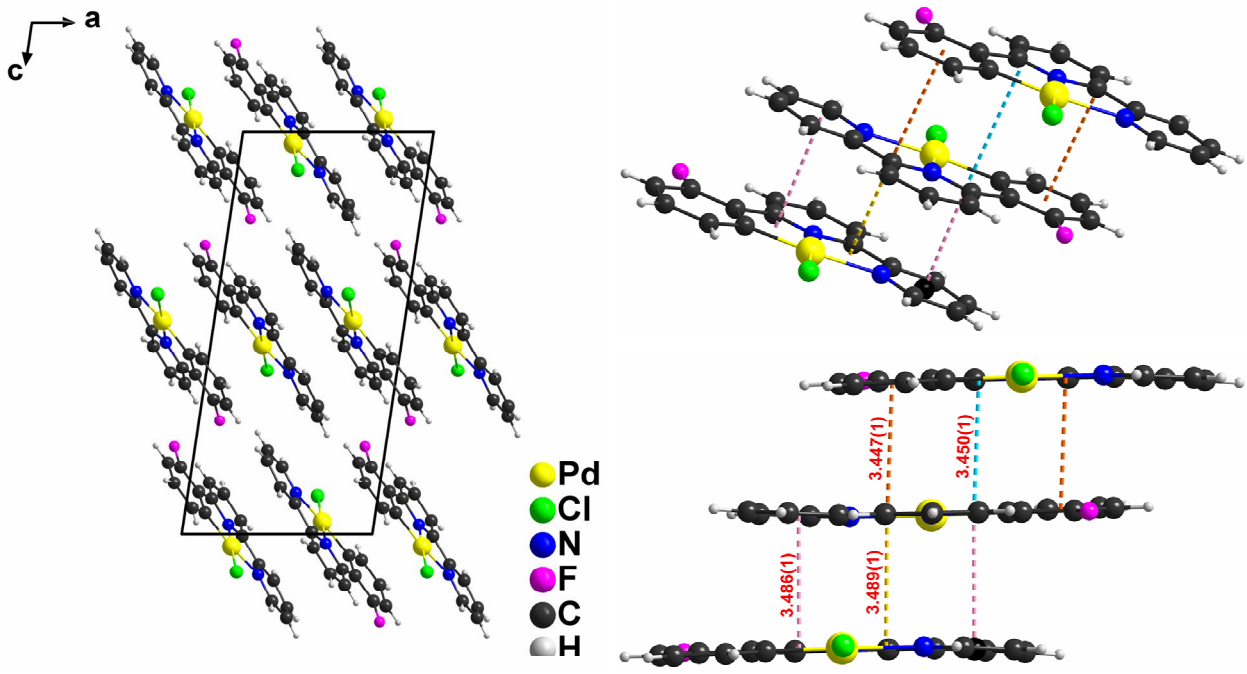

Fig. 2. Unit cell of [Pd(FPhbpy)Cl], viewed along the *b* axis (left) and details of the π stacking (right). Colour code; orange: 3.447(1) Å; cyan: 3.450(1) Å; pink: 3.486(1) Å; yellow: 3.489(1) Å.

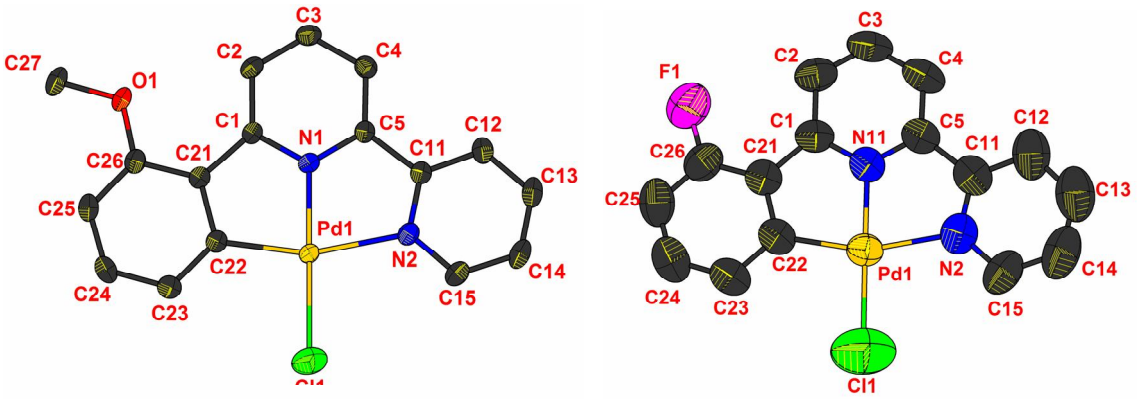

Fig. 3. Molecular structures from single crystal XRD of [Pd(MeOPhbpy)Cl] (left) und [Pd(FPhbpy)Cl] (right) both at 50% probability level with numbering; protons were omitted for clarity.

same is true for the phenyl H6Ph proton.

Crystal and Molecular Structures

Single crystals of [Pd(MeOPhbpy)Cl] (left) and [Pd(FPhbpy)Cl] were obtained from DMSO-d_6 solutions and the Unit cell and molecular structures (Fig. 2, Fig. 3 and Fig. S18) were determined with the results summarised in Table 1 (more data in Table S3).

The two compounds crystallise isostructural in the monoclinic space group *P* 2_1/c with four formula units in the

Table 1. Details of the Crystal Structure Determination and Selected Structural Data of [Pd(MeOPhbpy)Cl] and [Pd(FPhbpy)Cl][a] and the Reported Structure of [Pd(Phbpy)Cl]

	[Pd(MeOPhbpy)Cl]	[Pd(FPhbpy)Cl]	[Pd(Phbpy)Cl] [40]
Formulae	$C_{17}H_{13}N_2OPdCl$	$C_{16}H_{10}N_2FPdCl$	$C_{16}H_{11}N_2PdCl$
Molar weight	390.04 g mol^{-1}	381.03 g mol^{-1}	373.14 g mol^{-1}
Crystal system, space group	Monoclinic, $P\,2_1/c$	Monoclinic, $P\,2_1/c$	Monoclinic, $C2/c$
Cell	a = 8.800 Å	a = 8.360 Å	a = 10.578(2) Å
	b = 9.090 Å	b = 9.050 Å	b = 14.166(2) Å
	c = 18.030 Å	c = 17.950 Å	c = 9.016(1) Å
	β = 103.30°	β = 98.64°	β = 99.03(1)°
Volume, Z	1403.6 Å^3, 4	1342.6 Å^3, 4	1334.3 Å^3, 4
Calc. density	1.846 mg m^{-3}	1.885 mg m^{-3}	1.86 mg m^{-3}
F(000)	748	728	n.a.[b]
Coll., independ. reflections	12419, 2967	20053, 2899	2473/1091
R(int), GooF	0.0499, 1.092	0.1263, 0.983	n.a.[b]
R_1/wR_2 [$I > 2$ sigma(I)]	0.0254/0.0609	0.0377/0.0796	0.0241/0.0258
R_1/wR_2 (all data)	0.0271/0.0618	0.0744/0.0927	n.a.[b]
res. electrons and holes (eÅ^{-3})	0.478 and -0.836	0.516 and -0.615	n.a.[b]
CCDC	2026485	2026484	1194947
Distances (Å)			
Pd–N1, Pd–Cl1	1.953(2), 2.3215(6)	1.931(4), 2.281(2)	1.960(4), 2.316(2)
Pd–C22, Pd–N2	1.979(2), 2.138(2)	1.990(5), 2.130(4)	2.067(3)[c]
C5–C11, C1–C21	1.478(3), 1.461(3)	1.481(7), 1.458(7)	1.455(4)
C21–C22, C11–N2	1.423(3), 1.354(3)	1.380(7), 1.340(7)	1.387(4)[c]
Angles (°)			
N1–Pd–N2, N1–Pd–C22	79.42(7), 81.80(8)	79.7(2), 81.7(2)	80.3(1), 80.3(1)
N1–Pd–Cl1, N2–Pd–C22	177.43(5), 161.20(7)	179.1(2), 161.4(2)	180.0(1), 159.9(1)
Cl1–Pd–C22, Cl1–Pd–N2	98.29(6), 100.43(5)	98.8(1), 99.8(1)	99.7(1), 99.7(1)
Σ Angles around Pd	360	360	360

[a]Measured at 150(2) K at λ = 0.71073 Å. [b]Values not provided. [c]Structure solution in $C2/c$ without C/N discrimination. This is thus an averaged value.

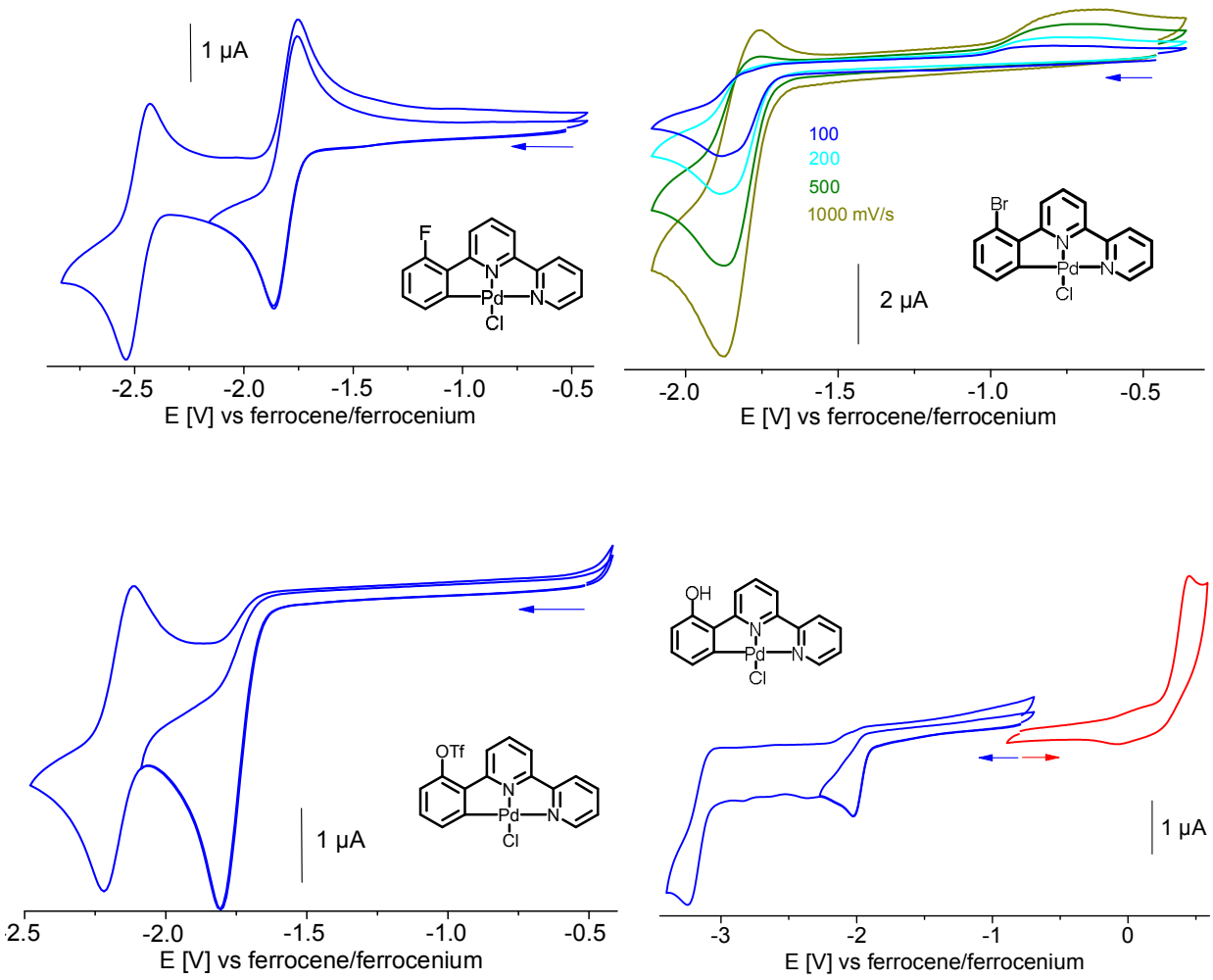

Fig. 4. Cyclic voltammograms of [Pd(XPhbpy)Cl] in 0.1 M *n*-Bu_4NPF_6/THF (tetrahydrofurane) at 298 K and 100 mV s^{-1} scan rate (if not otherwise given). Potentials in V *vs*. ferrocene/ferrocenium.

unit cell. The molecules stack in a head-to-tail fashion along the crystallographic *a* axis. Thus, the Pd atoms of two adjacent molecules get as close as 4.5432(5) Å (and 4.9024 Å; see Fig. 2) for [Pd(FPhbpy)Cl] and 3.4331(3) for the OMe derivative (Fig. S18).

The molecules show fully planar structures, while the angles around Pd are slightly distorted from ideal 90° (for square planar) due to the chelate bite angles of about 80° which are quite invariant for Pd(II) complexes of Phbpy or bpy units [32,34,37,40,47,70-72]. Both structures are quite similar to the previously reported "parent" complex [Pt(Phbpy)Cl] [40].

Electrochemical Experiments and Density Functional Theory (DFT) Calculations

All complexes [Pd(YPhbpy)Cl] exhibit two reduction waves in the ranges from –1.7 to –2.0 and –2.2 to –2.6 V (Fig. 4, 5, S19, S20, data in Table 2) and one oxidation wave in the range 0.5 to 1.0 V. Apart of these similarities, the Y substituent has an enormous impact on the reversibility and the potentials.

For the series of complexes [Pd(Phbpy)X] with X = Cl,

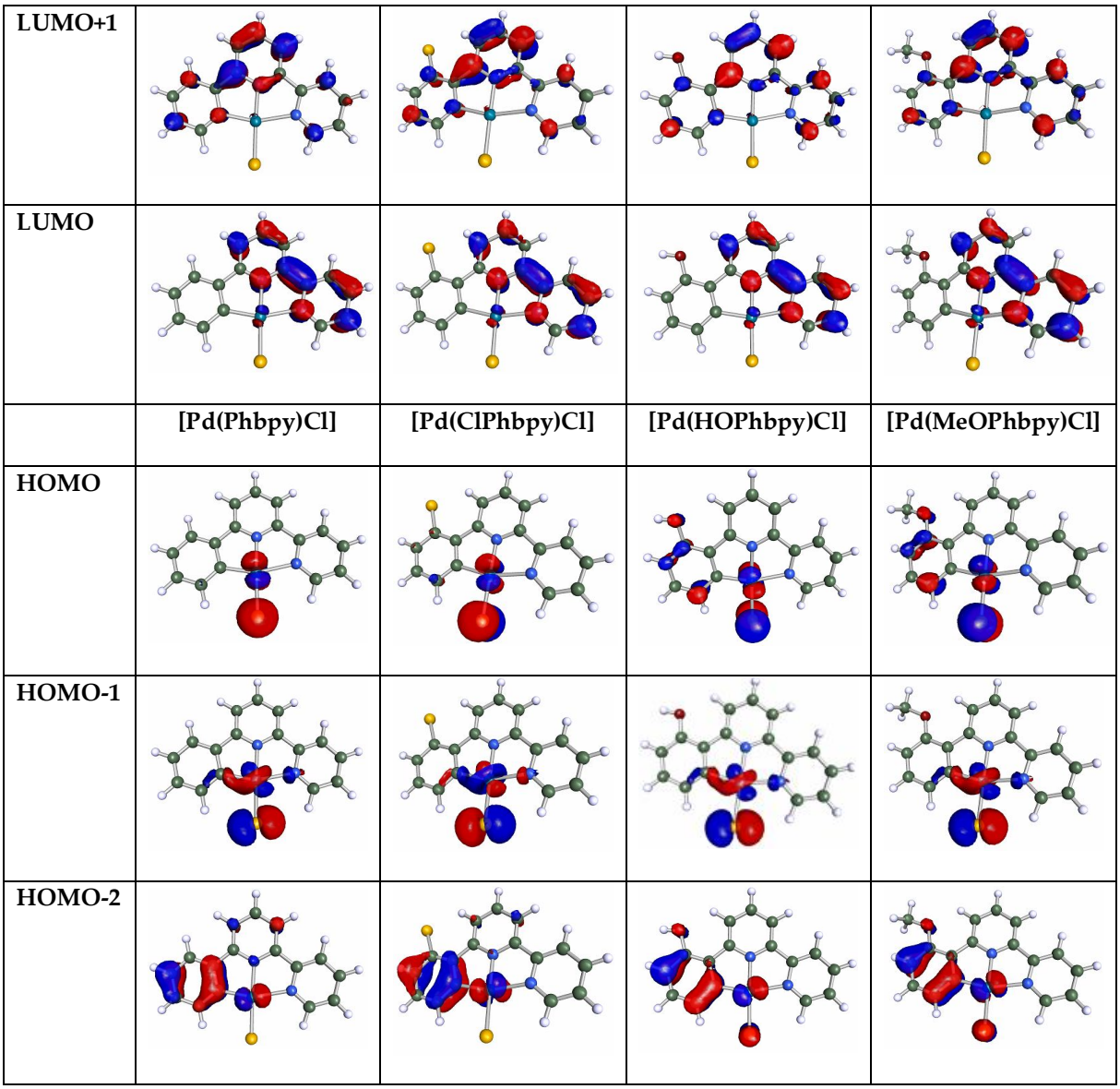

Fig. 5. DFT-calculated lowest unoccupied molecular orbitals (LUMO) and highest occupied molecular orbitals (HOMO) of [Pd(Phbpy)Cl], [Pd(ClPhbpy)Cl], [Pd(HOPhbpy)Cl] and [Pd(MeOPhbpy)Cl] (from left to right). Calculated on B3LYP level using def2-TZV(P) basis sets for C, H, N, O and LAN-L2DZ for Pd (ECP: Hay/Wadt (n-1) [78]). The isosurface is set to 0.05.

Br, I, the potentials of the two reversible reduction waves increase slightly by 0.06 V within the series Cl < Br < I, but the oxidation potential decrease markedly by almost 0.5 V. This is in line with a Phbpy ligand-centred reduction event and largely Pd–X centred oxidation. The electrochemical band gap decreases thus from 2.72 to 2.17 (from Cl to I). DFT calculations on [Pd(Phbpy)Cl] (Fig. 5) show a clearly bpy-centred lowest unoccupied molecular orbital (LUMO)

Table 2. Redox Potentials of Complexes [Pd(XPhbpy)Cl][a]

	$E_{1/2}$ (red2)	$E_{1/2}$ (red1)	E_{pa} (ox1)	ΔE (red1-red2)	ΔE (ox1-red1)	*DFT*[d]
[Pd(Phbpy)Cl)]	-2.60	-1.92	0.80[b]	0.68	2.72	3.58
[Pd(Phbpy)Br)]	-2.54	-1.89	0.63[b]	0.65	2.52	
[Pd(Phbpy)I)]	-2.51	-1.86	0.31[b]	0.65	2.17	
[Pd(FPhbpy)Cl)]	-2.48	-1.81	1.02	0.67	2.83	
[Pd(ClPhbpy)Cl)]	-2.50 irr	-1.69	1.05	0.81	2.74	3.59
[Pd(BrPhbpy)Cl)]	-2.57 irr	-1.83 irr	0.99	0.69	2.82	
[Pd(HOPhbpy)Cl)]	-3.25 irr	-2.00 irr	0.45	1.23	2.45	3.31
[Pd(MeOPhbpy)Cl)]	-2.58	-1.89	0.94	0.69	2.58	3.43
[Pd(TfOPhbpy)Cl)]	-2.16	-1.79 irr	1.13	0.35	2.92	
[Ni(Phbpy)Cl][c]	-2.60	-1.93	0.06 rev	0.67	1.99	
[Pt(Phbpy)Cl][c]	-2.48	-1.78	0.41	0.70	2.19	

[a]From cyclic voltammetry in *n*-Bu_4NPF_6/THF (tetrahydrofurane). Potentials in V *vs*. ferrocene/ferrocenium, half-wave potentials $E_{1/2}$ for reversible processes (rev), cathodic peak potentials E_{pc} for irreversible reductions (irr). [b]Measured in MeCN. [c]From ref. [77]. [d]DFT-calculated HOMO-LUMO gaps for the S_0 states.

and a highest occupied molecular orbital (HOMO) centred on Pd and the X coligand, what is fully in line with the electrochemical data. Substitution at the phenyl core for the complexes [Pd(YPhbpy)Cl] alters both reduction and oxidation potentials and HOMO-LUMO band gaps vary from 2.45 to 2.92. The DFT-calculated band gaps for the four complexes decrease along the series [Pd(ClPhbpy)Cl] > [Pd(ClPhbpy)Cl] > [Pd(MeOPhbpy)Cl] > [Pd(HOPhbpy)Cl] from 3.59 to 3.31 in agreement with the trend observed for the electrochemical gaps (Table 2).

Compared with the Ni and Pt complexes, the Pd derivative [Pd(Phbpy)Cl] has by far the highest oxidation potential and the ordering is Ni < Pt << Pd. A similar series was observed for the non-cyclometalated complexes [M(bpy)$(Mes)_2$] (Mes = 2,4,6-trimethylphenyl = mesityl with M = Ni (-0.14 V), Pt (0.45 V); Pd (0.57 V) [70,73,74] and very recently Ni, Pd and Pt complexes of a tetradentate dianionic thiosemicarbazone-based O^N^N^S ligand [75]. This trend agrees well with the second ionisation energy increasing along the series Ni (18.2 eV) < Pt (18.6 eV) << Pd (19.4 eV) and the electron binding energies of the valence p electrons (Ni: 66.2 eV, Pt 51.7 eV, Pd 50.9 eV [76].

The electrochemical responses to variations on the phenyl core of the Y–Phbpy ligand reveal multiple influence of the Y substituent. Firstly, if the Y group represents a good leaving group, the first reduction wave is irreversible, as observed for Y = Br, HO and TfO, while F, Cl and MeO derivatives show reversible first reduction waves. This observation is fully in line with the EC reaction generally observed for halogenated arenes. After electrochemical reduction (*E*), halides cleave in a chemical follow-up reaction (*C*) at a rate that is depending on their leaving group character, usually I > Br > Cl >> F. The same was observed for the protoligands YPhbpy (Figs. S13 and S14 in the Supplementary Information). Secondly, electron-withdrawing substituents Y cause a marked increase of the oxidation potentials and also to some extent to the reduction potentials (they render them less negative).

The DFT calculated lowest unoccupied molecular orbitals (LUMO) of some [Pd(YPhbpy)Cl] complexes are

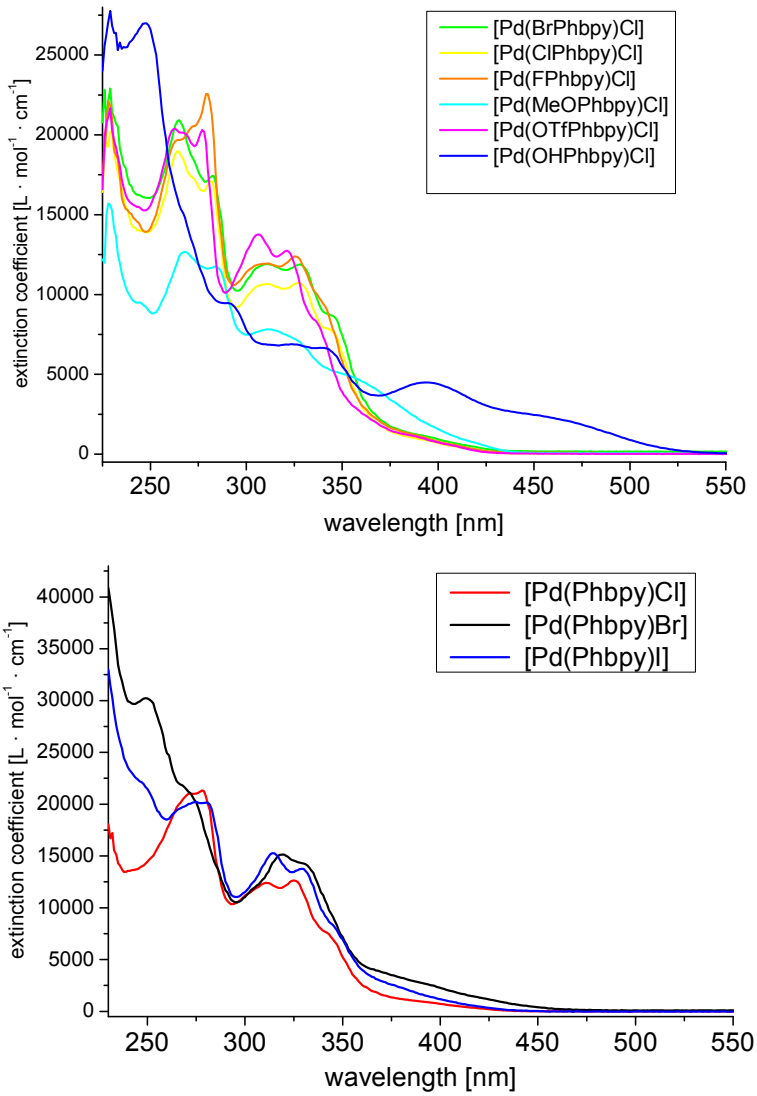

Fig. 6. UV-Vis absorption spectra of complexes [Pd(YPhbpy)Cl] (left) and [Pd(Phbpy)X] (X = Cl, Br, I) (right) in CH_2Cl_2.

largely centred on the 2,2'-bipyridine (bpy) unit with only marginal metal contribution. The LUMO+1 is also localised the on the bpy unit but obtains also small contributions from the phenyl group with coefficients on C2, C4 and C6. The highest occupied molecular orbitals (HOMO) are largely localised on the metal and the chloride coligand with the exception of [Pd(ClPhbpy)Cl] where a contribution of the Ph group to the HOMO was found. Marked contributions to HOMO-2 and HOMO-4 (not shown) come from the phenyl groups with high coefficients on all C atoms. The DFT-calculated orbital contributions are well consistent with the electrochemical data.

UV-Vis Absorption Spectroscopy, Time-dependent TD-DFT Calculations and Spectroelectrochemistry

The yellow colour of all complexes is due to the characteristic absorptions peaking around 320 nm and tailing down to about 430 nm observed in CH_2Cl_2 solution (Fig. 6

and S21, data in Tables 3 and S4). The intense and structured band system ranging from 250 to 300 nm is also observed in the protoligands YPhbpy (Fig. S5) and they can be assigned to π-π* or intraligand (IL) excitations. In the complexes they were followed by the structured band systems ranging from 300 to 350 nm. In view of previous studies on related cyclometalated Pd(II) [30,36,38,44-46] we assign them to excitations with mixed IL/Pd(d)-to-π*(ligand) or metal-to-ligand charge transfer (MLCT) character with a high IL component. The long-wavelength absorptions found as shoulders from 350 to 430 nm are assigned to similar excitations of mixed character, this time with essentially MLCT contributions.

The three complexes [Pd(Phbpy)X] with X = Cl, Br and I show very similar absorption spectra (Fig. 6, right), letting us assume that the coligand X does not markedly contribute to the visible and UV excitations. Very obviously, the hydroxo-substituted complex [Pd(HOPhbpy)Cl] and to a smaller extent also the methoxy derivative [Pd(MeOPhbpy)Cl] differ from the other complexes in that their long-wavelength absorptions are markedly red-shifted, for the OH complex maxima were found around 400 and 460 nm rendering this complex orange. This agrees with the lower electrochemically measured HOMO-LUMO gaps and the DFT-calculated HOMO-LUMO gaps for the S_0 ground state (Table 2). In order to gain more insight we embarked on TD-DFT calculations of the optical absorptions for these two complexes (Fig. 7, the [Pd(ClPhbpy)Cl] derivative and the parent complex [Pd(Phbpy)Cl], including both singlet and triplet excitations (Fig. 7 and 8, data in Tables S5 to S8).

For the parent complex [Pd(Phbpy)Cl] we obtained good agreement of the calculated with the experimental data (Fig. 7). Using the same methodology on the ClPhbpy derivative gave a rather poor match between the calculated spectrum and the experimental data. Especially, the calculations predicted red-shifted singlet excitations at 477 and 443 nm of reasonable strength caused by the substitution with Cl. But the experimental spectrum is largely the same as for the parent complex. Importantly, the high similarity of the absorption spectra of [Pd(Phbpy)Cl] and [Pd(ClPhbpy)Cl] is in good agreement with the electrochemical data of the two complexes. In contrast to this similarity, the DFT calculations showed a marked higher contribution of the Ph group to the HOMO for the ClPhbpy derivative (compare Fig. 5, the excited states composition is very similar) probably caused by the -I and +M effect of the Cl substituent and this lead obviously to the red-shift of the TD-DFT calculated long-wavelength bands. We assume that both calculations overestimate the substitution effects caused by Cl. Replacing the electron-withdrawing Cl through the electron-withdrawing HO and the electron-donating MeO group did not cause marked changes in the frontier orbital composition (compare Fig. 5) but allowed the reproduce quite well the absorption spectra of [Pd(HOPhbpy)Cl] and [Pd(MeOPhbpy)Cl] through TD-DFT calculations (Fig. 8). At the moment we can only speculate, that the incorporation of the light HO and MeO substituents are quite well adapted by the calculation method while the introduction of the heavier Cl atom was less successful. This calls for further DFT calculations using other combinations of basis sets and functionals as *e.g.* M06 (which includes dispersion). This will be done in near future.

Upon spectroelectrochemical reduction all complexes showed structured absorption bands at about 350, 420, 580 and 870 nm (Fig. 9, S22). Similar bands have been observed before for Phbpy complexes of Ni(II) and bpy complexes of Ni(II), Pd(II) and Pt(II) and were assigned to SOMO→LUMO (SOMO = singly occupied molecular orbital) excitations of the reduced complexes [56,58,70,73,74,79]. The appearance of these bands thus confirm that the target orbital for the reduction (LUMO) is essentially localised in the bpy moiety of the Phbpy ligand. The reduced complexes are thus best described as $[Pd(II)(YPhbpy^{\bullet-})X]^{\bullet-}$ and not as Pd(I) radical species. Small contributions of the metal or the Ph group can be estimated from the small changes of the absorption bands with the substitution pattern (Table 4). Also for the second reduction strong evidence is found for a bpy^{2-}-centred character of the long-wavelength absorptions.

CONCLUSIONS AND OUTLOOK

We were able to synthesise two series of organometallic Pd(II) complexes [Pd(YPhbpy)X] (X = Cl, Br, or I and Y = F, H, HO, MeO and TfO) and study the effects of the X coligand and the Y substituents on the structures, spectroscopy and electrochemical properties by a combined

Table 3. Selected UV-Vis Absorption Spectral Data of [Pd(YPhbpy)X][a]

	λ_1 (ε)	λ_2 (ε)	λ_3 (ε)	λ_4 (ε)	λ_5 (ε)	λ_6 (ε)
[Pd(Phbpy)Cl]	266 (20) sh	278 (21)	311 (12)	325 (13)	342 (8) sh	402 (1) sh
[Pd(Phbpy)Br]	266 (21) sh	281 (20)	314 (15)	329 (14)	345 (8) sh	402 (1) sh
[Pd(Phbpy)I]	249 (30)	269 (22)	319 (15)	330 (14) sh	345 (9) sh	395 (3) sh
[Pd(FPhbpy)Cl]	264 (20)	279 (26)	310 (12)	325 (12)	338 (10) sh	402 (1) sh
[Pd(ClPhbpy)Cl]	264 (19)	282 (17)	311 (11)	327 (11)	343 (8) sh	402 (1) sh
[Pd(BrPhbpy)Cl]	265 (21)	282 (17)	311 (12)	328 (12)	344 (9) sh	402 (1) sh
[Pd(TfOPhbpy)Cl]	262 (20)	277 (20)	306 (14)	321 (13)	334 (9)	402 (1) sh
[Pd(MeOPhbpy)Cl]	268 (13)	284 (12)	312 (8)	327 (7) sh	353 (5) sh	418 (1) sh
[Pd(HOPhbpy)Cl]	248 (27)	290 (10) sh	323 (7)	340 (7)	394 (5)	448 (3) sh
[Ni(Phbpy)Cl][b]	281		321	354	391	596
[Pt(Phbpy)Cl][b]	278	302	330	363	410	430

[a]Absorption maxima λ in nm in CH_2Cl_2 solution; molar absorption coefficient ε in 1000 mol^{-1} cm^{-1}. [b]From ref. [77].

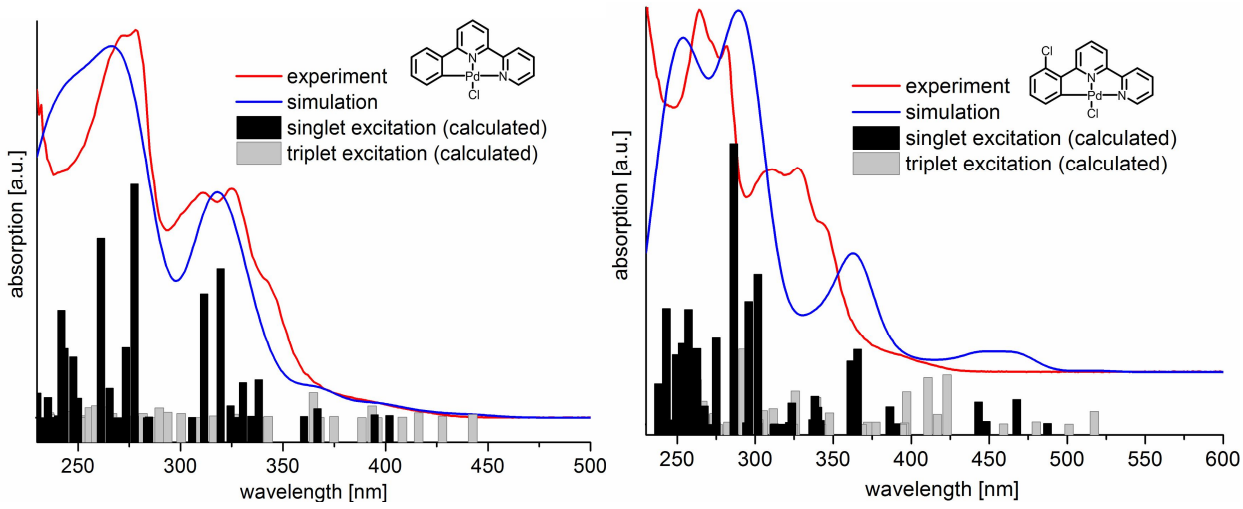

Fig. 7. TD-DFT-calculated (blue) und experimental (red) UV-Vis absorption spectrum of [Pd(Phbpy)Cl] (left) and [Pd(ClPhbpy)Cl] (right) in CH_2Cl_2 at 298 K. Verticals show calculated singlet (black) and triplet (grey) transitions, the blue line represents the convolute. Simulation on B3LYP level using def2-TZV(P) basis sets for C, H, N, O, LAN-L2DZ for Pd (ECP Hay/Wadt (n-1) [78]) and COSMO with ε = 8.93 (CH_2Cl_2).

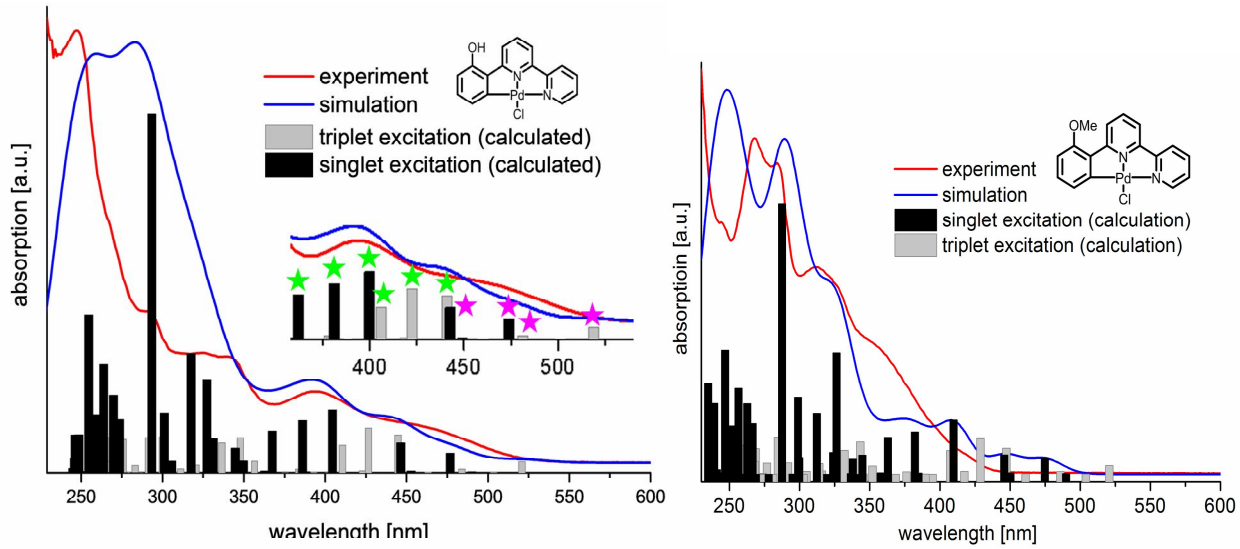

Fig. 8. TD-DFT-calculated (blue) und experimental (red) UV-Vis absorption spectrum of [Pd(HOPhbpy)Cl] (left) and [Pd(MeOPhbpy)Cl] (right) in CH_2Cl_2 at 298 K. Verticals show calculated singlet (black) and triplet (grey) transitions, the blue line represents the convolute. The coloured asterisks mark the same transition to allow comparison of singlet and triplet excitations. Simulation on B3LYP level using def2-TZV(P) basis sets for C, H, N, O, LAN-L2DZ for Pd (ECP Hay/Wadt (n-1) [78]) and COSMO with ε = 8.93 (CH_2Cl_2).

Table 4. UV-Vis Absorption Spectral Data of Reduced [Pd(Phbpy)X]$^{\bullet-}$ Complexes[a,b]

Reduced complexes	λ_1 (ε)	λ_2 (ε)	λ_3 (ε)	λ_4 (ε)
[Pd(Phbpy)Cl]$^-$	440	543	583	857
[Pd(FPhbpy)Cl]$^-$	437	533	573	877
[Pd(HOPhbpy)Cl$^-$]	426	541	581	882
[Pd(Phbpy)Br]$^-$	442	546	585	867
[Pd(Phbpy)I]$^-$	442	543	583	863
[Pd(bpy)(Mes)$_2$]$^{-c}$	-	397 (6.3)	537 (3.0)	817 (1.0)
[Ni(Phbpy)Br]$^{-d}$	296 (51.3)	376 (11.8)	593 (6.0)	1006 (1.3)
[Ni(bpy)(Mes)$_2$]$^{-e}$	-	355 (14.9)	530 (2.6)	940 (1.7)
Bpy^{-f}	-	398	585	1230

[a]Absorption maxima λ in nm; molar absorption coefficient ε in 1000 mol^{-1} cm^{-1}. [b]Generated by *in situ* electrolysis in 0.1 M *n*-Bu_4NPF_6/THF at ambient temperatures. [c]From ref. [70]. [d]From ref. [56]. [e]From ref. [73]. [f]From ref. [79].

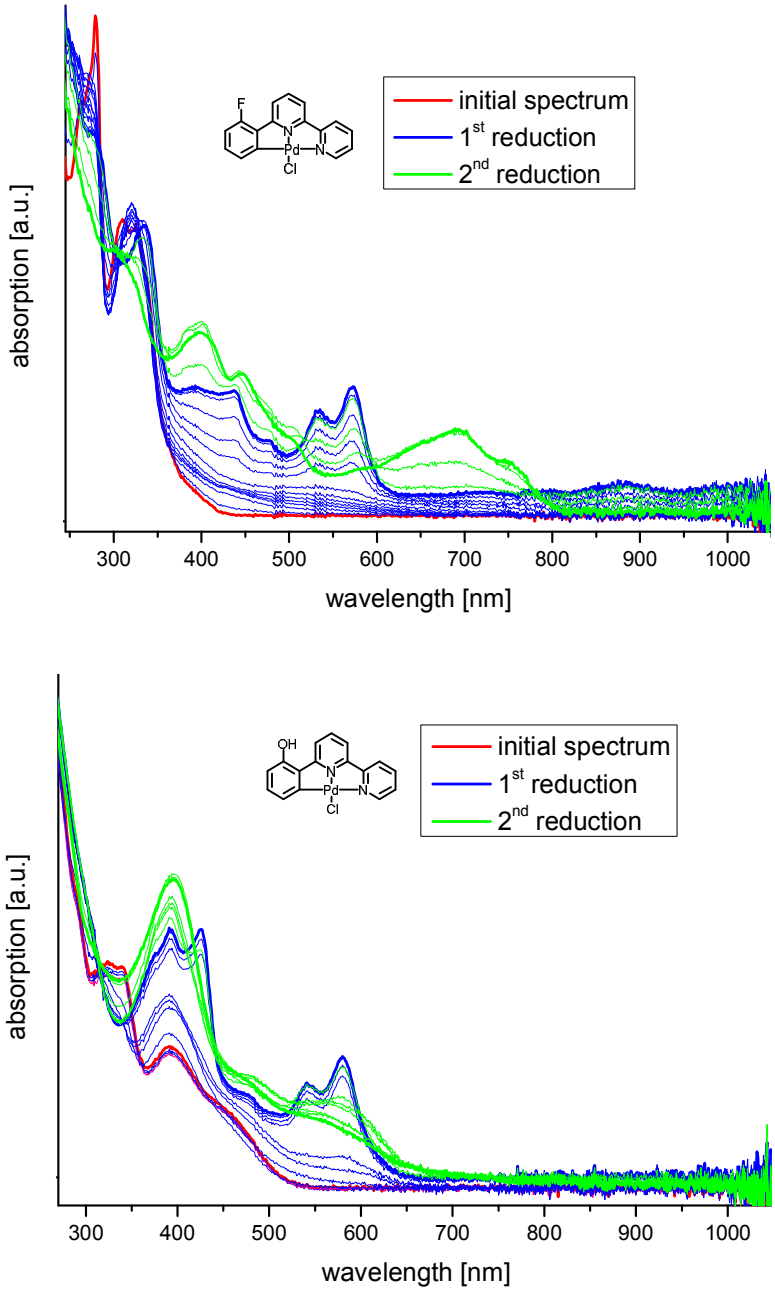

Fig. 9. UV-Vis absorption spectra of [Pd(FPhbpy)Cl] (left) und [Pd(HOPhbpy)Cl] (right) during electrochemical reduction in 0.1 M *n*-Bu_4NPF_6/THF.

experimental/theoretical (DFT-density functional theory) approach. The complexes of the unsubstituted tridentate anionic and cyclometalating C^N^N ligand 6-(phen-2-ide)-2,2'-bipyridine (⁻Phbpy) were formed through oxidative addition of the protoligands X–Phbpy (X = Cl, Br and I) with [$Pd_2(dba)_3$] tris(dibenzylideneacetone)dipalladium(0) in yields ranging from 23 to 51%. Complexes [Pd(YPhbpy)Cl] with the substituted YPhbpy ligand resulted from C–H

palladation of the same protoligands or the derivatives Y–Phbpy with Y = F, H, HO, MeO and TfO) with K_2PdCl_4 in yields ranging from 52 to 98%. All protoligands and Pd(II) complexes were fully characterised using MS, NMR and single crystal XRD for Y = F, MeO. Two reversible electrochemical reductions were found for the [Pd(Phbpy)X] complexes, while for the YPhbpy derivatives *EC* behaviour was observed with a rapid cleavage of Y^- (*C* = chemical reaction) following the electrochemical reduction (*E*) for Y representing good leaving groups (Br, HO and TfO, but not F, Cl and MeO). The potentials of these reduction showed large variations upon Y substitution but are less sensitive to the exchange of the X coligands. In contrast, the largely irreversible oxidations are quite sensitive to variations of X. These finding, together with DFT calculations on the frontier orbitals and UV-Vis absorption spectroelectrochemistry are in keeping with mainly bpy-centred reduction and oxidation with essential Pd and X contributions. TD-DFT-calculated UV-Vis absorption spectra are in good agreement with experimental spectra for the parent [Pd(Phbpy)Cl] and the complexes containing HOPhbpy and MeOPhbpy which show a marked red-shift of the long-wavelength metal-to-ligand charge transfer (MLCT) bands. TD-DFT calculations on the ClPhbpy derivative were less successful. The calculations also predicted long-wavelength absorptions as for the HO and MeO derivatives but the experimental absorptions are very similar to the unsubstituted parent complex [PdPhbpy)Cl]. Remarkably, the incorporation of all three ligands HO, MeO and Cl into the DFT calculations, using the same basis sets gave very good agreement with the electrochemical data. We assume thus, that the used TD-DFT methodology is unsuitable to model properly the effect of the heavier Cl atom. In future calculations we will vary thus the method and basis sets to shed light on this phenomenon.

EXPERIMENTAL

General

All complex preparations and measurement were carried out in a dry argon atmosphere using Schlenk techniques. Solvents (THF, toluene, diethyl ether and MeCN) were dried using a MBRAUN MB SPS-800 solvent purification system (MBRAUN, Garching, Germany). THF was further purified over an alloy of sodium and potassium.

Instrumentation

NMR spectra were recorded using a Bruker (Bruker, Rheinstetten, Germany) Avance II 300 MHz spectrometer (^{1}H: 300.13 MHz, ^{13}C: 75.47 MHz, ^{19}F: 282 MHz) using a triple resonance ^{1}H, ^{19}F, BB inverse probehead. The unambiguous assignment of the ^{1}H and ^{13}C resonances was obtained from ^{1}H TOCSY (TOtal Correlated SpectroscopY), ^{1}H COSY (COrrelated SpectroscopY), ^{1}H NOESY (Nuclear Overhauser Enhancement SpectroscopY), gradient selected ^{1}H, ^{13}C HSQC (Heteronuclear Single Quantum Coherence) and HMBC (Heteronuclear Multiple Bond Correlation) experiments. All 2D NMR experiments were performed using standard pulse sequences from the Bruker pulse program library. Chemical shifts were relative to TMS for ^{1}H and ^{13}C and relative to CCl_3F or trifluoromethylbenzene for ^{19}F. The spectra analyses were performed using *Bruker TopSpin 2* software. Elemental analyses were carried out using a Hekatech CHNS EuroEA 3000 Analyzer (Hekatech, Wegberg, Germany). EI-MS spectra were measured at 20 mV positive ionisation energy with a Finnigan MAT 900 S (Finnigan Mat, Bremen, Germany). Simulations were performed using ISOPRO 3.0. Electrochemical experiments were carried out in 0.1 M *n*-Bu_4NPF_6 solutions using a three-electrode configuration (glassy carbon electrode, Pt counter electrode, Ag/AgCl reference) and an Autolab PGSTAT30 potentiostat and function generator (Metrohm, Filderstadt, Germany). Data were processed using GPES 4.9 (General Electrochemical System Version 4.9). The ferrocene/ferrocenium couple served as internal reference. Spectroelectrochemical investigations (UV-Vis) were performed at ambient temperature using an OTTLE (optical transparent electrochemical) cell [80,81]. UV-Vis absorption spectra were recorded using Varian Cary50 Scan or Cary05E photospectrometers (Varian, Darmstadt, Germany).

Crystal Structure Determination

The data collection was performed at T = 100(2) K on a *STOE IPDS II* diffractometer (STOE and Cie., Darmstadt, Germany) with Mo-Kα radiation (λ = 0.71073 Å) employing ω-φ-2θ scan technique. The structures were solved by dual space methods (SHELXT-2015) [82] and refined by full-matrix least-squares techniques against F^2 (SHELXL-2017/1) [83,84] with $F_0^2 \geq 2\sigma(F_0^2)$ with the results shown in Table 1 (and Supplementary Data). The numerical

absorption corrections (X-RED V1.31; STOE and Cie, 2005) [85] were performed after optimising the crystal shapes using X-SHAPE V1.06 (Stoe & Cie, 1999) [86]. All non-hydrogen atoms were treated anisotropically; hydrogen atoms were included by using appropriate riding models. CCDC 2026485 [Pd(MeOPhbpy)Cl] and 2026484 [Pd(FPhbpy)Cl] contains the full crystallographic data. This data can be obtained free of charge at www.ccdc.cam.ac.uk/conts/retrieving.html or from the Cambridge Crystallographic Data Centre, 12 Union Road, Cambridge, CB2 1EZ UK. Fax: +44-1223-336-033; Email: deposit@ccdc.cam.ac.uk.

DFT Calculations

Quantum chemical calculation based on the density functional theory (DFT) were carried out using the „resolution of identity" Coulomb approximation [87,88] in the program package TURBOMOLE [89] under the TMoleX [90] platform. Molecular structures for [Pd(Phbpy)Cl], [Pd(ClPhbpy)Cl], [Pd(MeOPhbpy)Cl] and [Pd(HOPhbpy)Cl] were first geometry-optimised using the double-ξ-valence basis set def-SV(P) [91] and further optimised using the triple-ξ-valence basis set def2-TZVP [92]. The resulting molecular metrics were checked for consistency within these four structure and also match well to the experimental structural data of [Pd(Phbpy)Cl] [40] and [Pd(MeOPhbpy)Cl]. Time-dependent TD-DFT calculations were carried out using the basis set def2-TZVP and the solvent CH_2Cl_2 was included using COSMO [93,94] (conductor-like screening model); ε for CH_2Cl_2 is 8.93 [95]. Starting from geometry optimisation UV-Vis simulations were performed on B3LYP level [96-98] using def2-TZV(P) basis sets for C, H, N, O and LAN-L2DZ for Pd using effective core potentials (ECP) (n-1) by Hay and Wadt [78,99,100].

Reagents

$[Pd_2(dba)_3]$ was purchased from Acros Organics. All chemicals were purchased by commercial suppliers and were used without further purification.

Synthesis of Ligand Precursor and Protoligands H–Phbpy and X/Y–Phbpy

The 6-phenyl-2,2'-bipyridine precursor H–Phbpy was prepared through slight variation of an established procedure [59]. The protoligands Y/X–Phbpy with Y = F, Cl, Br, I, HO, MeO and triflate (TfO) were synthesis as outlined in the Supplementary Information through the *Kröhnke* method.

Synthesis of the Pd Complexes

Synthesis through oxidative addition using tris(dibenzylideneacetone)dipalladium(0)-general procedure. The purple solution of one equivalent tris(dibenzylideneacetone)dipalladium(0) $[Pd_2(dba)_3]$ two equivalents of the free protoligand in dry toluene was stirred at 60 °C for 150 min. The resulting green suspension was allowed to cool down to room temperature. The solid was filtered off and dissolved in $CHCl_3$. The resulting solution was washed two times with water and once with concentrated aqueous NaY solution. After removing the solvent under reduced pressure, the yellow solid was dried in vacuum.

6-(Phen-2-ide)-2,2'-bipyridine)chloridopalladium(II) [Pd(Phbpy)Cl]. From 212 mg (0.23 mmol) $[Pd_2(dba)_3]$, 123 mg (0.46 mmol) 6-(2-chlorophenyl)-2,2'-bipyridine, 20 mL dry toluene, 80 mL $CHCl_3$, 40 mL portions of water and brine. Yield: 80.7 mg (2.16 mmol, 47%). Anal. Calcd. $C_{16}H_{11}ClN_2Pd$ (M_W = 373.14 g mol^{-1}): C, 51.50; H, 2.97; N, 7.51%. Found: C, 51.12; H, 3.01; N, 7.50%. ^{1}H NMR (300 MHz, DMSO-d_6): δ = 8.63 (dd, 1H, J = 5.1, 0.9 Hz), 8.49 (d, 1H, J = 8.0 Hz), 8.24 (ddd, 2H, J = 7.7, 6.8, 1.3 Hz), 8.15 (t, 1H, J = 7.9 Hz), 8.00 (dd, 1H, J = 7.8, 1.0 Hz), 7.78 (ddd, 1H, J = 7.6, 5.2, 1.1 Hz), 7.65-7.60 (m, 1H), 7.54-7.49 (m, 1H), 7.13-7.04 (m, 2H) ppm. ^{13}C NMR (75 MHz, DMSO-d_6): δ = 164.06, 155.66, 154.63, 154.03, 149.53, 148.54, 140.94, 140.69, 136.63, 130.13, 127.98, 125.22, 125.12, 123.69, 120.42, 120.34 ppm. EI-MS(+) (20 eV): m/z = 374 $[M]^+$, 462 $[bpyPh\text{-}Phbpy]^+$, 337 $[M\text{-}Cl]^+$, 231 $[Phbpy]^+$.

6-(Phen-2-ide)-2,2'-bipyridine)bromidopalladium(II) [Pd(Phbpy)Br]. From 195.7 mg (0.21 mmol) $[Pd_2(dba)_3]$, 133 mg (0.42 mmol) 6-(2-bromophenyl)-2,2'-bipyridine, 30 mL dry toluene, 30 mL CH_2Cl_2 (instead of $CHCl_3$), 20 mL portions of H_2O and concentrated NaBr solution. Subsequent recrystallisation from 15 mL toluene was necessary to obtain the pure yellow product. Yield: 41 mg (0.01 mmol, 23%). Anal. Calcd. $C_{16}H_{11}N_2PdBr$ (M_W = 417.60 g mol^{-1}): 46.02; H, 2.66; N, 6.71%. Found: C,

46.05; H, 2.76; N, 6.71%. ^{1}H NMR (300 MHz, DMSO-d_6): δ = 8.80 (d, 1H, J = 4.4 Hz), 8.52 (d, 1H, J = 8.0 Hz), 8.25 (dd, 2H, J = 7.0, 1.3 Hz), 8.20 (t, 1H, J = 7.8 Hz), 8.05 (dd, 1H, J = 7.7, 1.2 Hz), 7.83-7.73 (m, 2H), 7.67 (dd, 1H, J = 7.4, 1.7 Hz), 7.15-7.00 (m, 2H) ppm. EI-MS(+) (20 eV): m/z = 418 $[M]^+$, 462 $[bpyPh\text{-}Phbpy]^+$, 337 $[M–Br]^+$, 232 $[HPhbpy]^+$.

6-(Phen-2-id)-2,2'-bipyridine)iodidopalladium(II) [Pd(Phbpy)I]. From 193 mg (0.21 mmol) $[Pd_2(dba)_3]$, 151.6 mg (0.42 mmol) 6-(2-iodophenyl)-2,2'-bipyridine, 30 mL dry toluene, 200 mL CH_2Cl_2 (instead of $CHCl_3$), 50 mL portions of H_2O and concentrated KI solution. Subsequent recrystallisation from 15 mL toluene was necessary to obtain the pure yellow product. Yield: 100 mg (0.22 mmol, 51%). Anal. Calcd. $C_{16}H_{11}N_2PdI$ (M_W = 464.60 g mol^{-1}): C, 41.36; H, 2.39; N, 6.03%. Found: C, 41.31; H, 2.38; N, 5.97%. ^{1}H NMR (300 MHz, DMSO-d_6): δ = 9.02 (d, 1H, J = 4.3 Hz), 8.52 (d, 1H, J = 8.0 Hz), 8.30-8.17 (m, 3H), 8.12 (d, 1H, J = 7.7 Hz), 8.06 (dd, 1H, J = 7.3, 1.7 Hz), 7.80-7.72 (m, 1H), 7.68 (dd, 1H, J = 7.6, 1.4 Hz), 7.13-7.04 (t, 1H), 6.97 (td, 1H, J = 7.6, 1.5 Hz) ppm. EI-MS(+) (20 eV): m/z = 464 $[M]^+$, 337 $[M–I]^+$, 232 $[Phbpy]^+$.

Synthesis through C–H activation-general description. Applying a modification of the Constable method [39,40], in a typical reaction 1 mmol Y–Phbpy and 326.4 mg (1 mmol) $K_2[PdCl_4]$ were dissolved in 60 mL of a 1:1 mixture of MeCN and water and stirred under reflux for 18 h. The yellow suspension filtered over a Büchner funnel. After washing the material with small amounts of H_2O, MeCN and *n*-pentane, the yellow solids were dried in vacuum.

6-(Phen-2-ide)-2,2'-bipyridine)chloridopalladium(II) [Pd(Phbpy)Cl]. From 93.50 mg (0.35 mmol) 6-(2-chlorophenyl)-2,2'-bipyridine and 131.40 mg (0.4 mmol) $K_2[PdCl_4]$, 10 mL H_2O and 10 mL MeCN. Yield: 116.50 mg (0.31 mmol, 78%). Anal. Calcd. $C_{16}H_{11}ClN_2Pd$ (M_W = 373.14 g mol^{-1}): C, 51.50; H, 2.97; N, 7.51%. Found: C, 51.12; H, 3.05; N, 7.50%. ^{1}H NMR (300 MHz, DMSO-d_6): δ = 8.63 (dd, 1H, J = 5.1, 0.9 Hz), 8.49 (d, 1H, J = 8.0 Hz), 8.24 (ddd, 2H, J = 7.7, 6.8, 1.3 Hz), 8.15 (t, 1H, J = 7.9 Hz), 8.00 (dd, 1H, J = 7.8, 1.0 Hz), 7.78 (ddd, 1H, J = 7.6, 5.2, 1.1 Hz), 7.65-7.60 (m, 1H), 7.54-7.49 (m, 1H), 7.13-7.04 (m, 2H) ppm. ^{13}C NMR (75 MHz, DMSO-d_6): J = 7.6, 5.2, 1.1 Hz), 7.65-7.60 (m, 1H), 7.54-7.49 (m, 1H), 7.13-7.04 (m, 2H) ppm. ^{13}C NMR (75 MHz, DMSO-d_6): δ = 164.06, 155.66, 154.63, 154.03, 149.53, 148.54, 140.94, 140.69, 136.63, 130.13, 127.98, 125.22, 125.12, 123.69, 120.42, 120.34 ppm. EI-MS(+) (20 eV): m/z = 374 $[M]^+$, 462 $[bpyPh\text{-}Phbpy]^+$, 337 $[M–Cl]^+$, 231 $[Phbpy]^+$.

6-(3-Chlorophen-2-ide)-2,2'-bipyridine)chloride-palladium(II) [Pd(ClPhbpy)Cl]. From 266.7 mg (1 mmol) 6-(2-chlorophenyl)-2,2'-bipyridine and 326.4 mg (1 mmol) $K_2[PdCl_4]$. Yield: 377.84 mg (0.98 mmol, 98%). Anal. Calcd. $C_{16}H_{10}N_2Cl_2Pd$ (M_W = 407.59 g mol^{-1}): C, 47.15; H, 2.47; N, 6.87%. Found: C, 47.16; H, 2.35; N, 6.88%. ^{1}H NMR (600 MHz, DMSO-d_6): δ = 8.65 (d, 1H, J = 6.1 Hz), 8.63 (d, 1H, J = 8.8 Hz), 8.52 (d, 1H, J = 8.1 Hz), 8.34 (d, 1H, J = 7.5 Hz), 8.27 (td, 1H, J = 7.8 Hz), 8.23 (t, 1H, J = 8.2 Hz), 7.83-7.78 (m, 1H), 7.64 (dd, 1H, J = 7.5 Hz), 7.18 (dd, 1H, J = 7.9 Hz), 7.07 (t, 1H, J = 7.7 Hz) ppm. EI-MS(+) (20 eV): m/z = 408 $[M]^+$, 373 $[M–Cl]^+$, 266 $[ClPhbpy]^+$, 231 $[Phbpy]^+$.

6-(3-Fluorophen-2-ide)-2,2'-bipyridine)chloride-palladium(II) [Pd(FPhbpy)Cl]. From 128.15 mg (0.51 mmol) 6-(2-fluorphenyl)-2,2'-bipyridine and 168.93 mg (0.52 mmol) $K_2[PdCl_4]$, 12 mL H_2O and 12 mL MeCN. Yield: 155 mg (0.40 mmol, 78%). Anal. Calcd. $C_{16}H_{10}N_2FPdCl$ (M_W = 391.14 g mol^{-1}): C, 49.13; H, 2.58; N, 7.16%. Found: C, 49.06; H, 2.54; N, 7.14%. ^{1}H NMR (600 MHz, DMSO-d_6): δ = 8.63 (d, 1H, J = 5.0 Hz), 8.50 (d, 1H, J = 8.0 Hz), 8.28 (td, 2H, J = 8.1 Hz), 8.20 (t, 1H, J = 8.1 Hz), 7.93 (d, 1H, J = 8.2 Hz), 7.80 (ddd, 1H, J = 7.6 Hz), 7.39 (d, 1H, J = 7.5 Hz), 7.19-7.10 (m, 1H), 6.95 (dd, 1H, J = 12.1 Hz) ppm. EI-MS (70 eV): m/z = 391 $[M]^+$, 357 $[M–Cl]^+$.

6-(3-Bromophen-2-ide)-2,2'-bipyridine)chloride-palladium(II) [Pd(BrPhbpy)Cl]. From 311.18 mg (1 mmol), 6-(2-Bromphenyl)-2,2'-bipyridine, 326.43 mg (1 mmol) $K_2[PdCl_4]$, 25 mL H_2O and 25 mL MeCN. Yield: 379.71 mg (0.84 mmol, 84%); Anal. Calcd. $C_{16}H_{10}N_2BrPdCl$ (M_W = 452.04 g mol^{-1}): C, 42.51; H, 2.23; N, 6.20%. Found: C, 42.83; H, 2.19; N, 6.20%. ^{1}H NMR (600 MHz, DMSO-d_6): δ = 8.83 (d, 1H, J = 8.4 Hz), 8.66 (dd, 1H, J = 5.3 Hz), 8.53 (d, 1H, J = 8.0 Hz), 8.38 (d, 1H), 8.34-8.20 (m, 2H), 7.87-7.77 (m, 1H), 7.71 (dd, 1H, J = 7.5 Hz), 7.39 (dd, 1H, J = 7.9 Hz), 6.98 (t, 1H, J = 7.7 Hz) ppm. EI-MS (70 eV): m/z = 452 $[M]^+$, 417 $[M–Cl]^+$, 372 $[M–Br]^+$, 337 $[M–Br–Cl]^+$.

6-(3-Hydroxyphen-2-ide)-2,2'-bipyridine)chloride-palladium(II) [Pd(HOPhbpy)Cl]. From 128.63 mg (0.52 mmol) 6-(2-hydroxyphenyl)-2,2'-bipyridine, 169.12 mg (0.52 mmol) $K_2[PdCl_4]$, 10 mL H_2O and 10 mL MeCN. Yield: 195.61 mg (0.50 mmol, 97%); Anal. Calcd. $C_{16}H_{11}N_2OPdCl$ (M_W = 389.15 g/mol): C, 49.38; H, 2.85; N, 7.20%. Found: C, 49.55; H, 2.86; N, 7.12%. ^{1}H NMR (600 MHz, DMSO-d_6): δ = 9.11 (d, 1H, J = 5.6 Hz), 8.60 (d, 1H), 8.57 (d, 1H), 8.48 (dd, 1H, J = 7.8 Hz), 8.35 (t, 1H, J = 8.4 Hz), 8.31 (td, 1H, J = 7.8 Hz), 8.03 (dd, 1H, J = 8.4 Hz), 7.77 (t, 1H, J = 7.3 Hz), 7.27 (t, 1H, J = 8.4 Hz), 7.00 (dd, 1H, J = 8.4 Hz), 6.74 (t, 1H, J = 8.2 Hz) ppm. ^{13}C NMR (151 MHz, DMSO-d_6): δ = 162.2, 156.6, 155.2, 151.3, 150.9, 140.7, 139.9, 132.5, 130.2, 127.3, 125.1, 123.9, 121.9, 120.6, 120.5, 116.2 ppm.

6-(3-Methoxyphen-2-ide)-2,2'-bipyridine)chloride-palladium(II) [Pd(MeOPhbpy)Cl]. From 130 mg (0.5 mmol) 6-(2-methoxyphenyl)-2,2'-bipyridine, 161.76 mg (0.5 mmol) $K_2[PdCl_4]$, 15 mL H_2O and 15 mL MeCN. Yield: 180 mg (0.45 mmol, 89%); Anal. Calcd. $C_{17}H_{13}N_2OPdCl$ (M_W = 403.17 g mol^{-1}): C, 50.64; H, 3.25; N, 6.95%. Found: C, 50.55; H, 3.22; N, 6.92%. ^{1}H NMR (600 MHz, DMSO-d_6): δ = 8.60 (d, 1H, J = 5.1 Hz), 8.43 (d, 1H, J = 8.0 Hz), 8.27-8.17 (m, 2H), 8.14 (d, 1H, J = 8.0 Hz), 8.07 (t, 1H, J = 8.0 Hz), 7.74 (t, 1H, J = 7.6 Hz), 7.18 (d, 1H, J = 7.4 Hz), 7.02 (t, 1H, J = 7.9 Hz), 6.76 (d, 1H, J = 8.3 Hz), 3.88 (s, 3H) ppm. EI-MS (70 eV): m/z = 403 $[M]^+$, 378 $[M–Cl]^+$.

6-(3-Triflatophen-2-ide)-2,2'-bipyridine)chloride-palladium(II) [Pd(TfOPhbpy)Cl]. From 340 mg (0.5 mmol) 6-(2-triflatophenyl)-2,2'-bipyridine, 190.17 mg (0.5 mmol) $K_2[PdCl_4]$, 15 mL H_2O and 15 mL MeCN. Yield: 136.8 mg (0.26 mmol, 52%); Anal. Calcd. $C_{17}H_{10}N_2F_3O_3SPdCl$ (M_W = 521.20 g mol^{-1}): C, 39.18; H, 1.93; N, 5.37; S, 6.15%. Found: C, 39.24; H, 1.90; N, 5.40; S, 6.18%. ^{1}H NMR (600 MHz, DMSO-d_6): δ = 8.66 (d, 1H, J = 4.2 Hz), 8.55 (d, 1H, J = 8.0 Hz), 8.40 (d, 1H, J = 7.8 Hz), 8.35 (t, 1H, J = 8.1 Hz), 8.30 (td, 1H, J = 7.8 Hz), 7.98 (d, 1H, J = 8.1 Hz), 7.83 (ddd, 1H, J = 7.7 Hz), 7.73 (dd, 1H, J = 7.6 Hz), 7.30 (t, 1H, J = 7.9 Hz), 7.19 (d, 1H, J = 8.2 Hz) ppm. ^{19}F NMR (282 MHz, DMSO-d_6): δ = -72.8 ppm. EI-MS (70 eV): m/z = 521 $[M]^+$, 388 $[M–SO_2CF_3]^+$.

AUTHOR CONTRIBUTIONS

R.v.d.S. co-designed the project and carried out the syntheses, all measurements and DFT calculations. S.S. refined the crystal structures, managed the data and provided figures. A.K. designed and supervised the project and wrote the manuscript. All authors have read and agreed to the submitted version of the manuscript.

FUNDING

The Deutsche Forschungsgemeinschaft [DFG Priority Programme 2102 "Light-controlled Reactivity of Metal Complexes"] KL1194/16-1 (AK) is acknowledged for funding of this project. AK also thanks the German Academic Exchange Service (DAAD) for a short-term short-time guest lectureship KD-0001052598-2 and the University of Shiraz, Iran for support.

ACKNOWLEDGMENTS

We are indebted to Dr. Ingo Pantenburg (Centre for XRD) for XRD measurements, to Dr. Nils Schlörer (Centre for NMR Spectroscopy) for help with the NMR data collection and Prof. Dr. Mathias Schäfer and Astrid Baum, Centre for Mass Spectrometry) for collecting MS data (all in the Department of Chemistry, University of Cologne). Fabian Malzbenden (MSc. Chem.) is acknowledged for help with the syntheses.

CONFLICTS OF INTEREST

The authors declare no conflict of interest.

APPENDIX

Supplementary Information

Supplementary Information related to this article can be found at http://dx.doi.org/xxx

Syntheses of precursors and protoligands were provided. Figures showing NMR spectra of the X/Y–Phbpy protoligands and the Pd complexes, crystal structures of [BrPhbpyH]Cl·2H_2O, [Pd(MeOPhbpy)Cl], and [Pd(FPhbpy)Cl], cyclic voltammogramms of protoligands

and complexes, UV-Vis absorption spectra of protoligands and complexes, including spectroelectrochemical UV-Vis spectra are presented. Supplementary tables with detailed UV-Vis absorption, electrochemical, structural of protoligands and complexes are provided together with tables containing DFT calculated data.

REFERENCES

[1] S. Rej, Y. Ano, N. Chatani, Chem. Rev. 120 (2020) 1788.

[2] R.A. Alharis, C.L. McMullin, D.L. Davies, K. Singh, S.A. Macgregor, Faraday Discuss 220 (2019) 386.

[3] P. Gandeepan, T. Müller, D. Zell, G. Cera, S. Warratz, L. Ackermann, Chem. Rev. 119 (2019) 2192.

[4] J.A. Harrison, A.J. Nielson, M.A. Sajjad, P. Schwerdtfeger, Organometallics 38 (2019) 1903.

[5] J.C.K. Chu, T. Rovis, Angew. Chem., Int. Ed. 57 (2018) 62.

[6] C. Sambiagio, D. Schönbauer, R. Blieck, T. Dao-Huy, G. Pototschnig, P. Schaaf, T. Wiesinger, M.F. Zia, J. Wencel-Delord, T. Besset, B.U.W. Maes, M. Schnürch, Chem. Soc. Rev. 47 (2018) 6603.

[7] D.L. Davies, S.A. Macgregor, C.L. McMullin, Chem. Rev. 117 (2017) 8649.

[8] J. He, M. Wasa, K.S.L. Chan, Q. Shao, J.-Q. Yu, Chem. Rev. 117 (2017) 8754.

[9] Y.-N. Ma, S.-X. Li, S.-D. Yang, Acc. Chem. Res. 50 (2017) 1480.

[10] J. Le Bras, J. Muzart, Eur. J. Org. Chem. (2017) 3528.

[11] N. Della Ca', M. Fontana, E. Motti, M. Catellani, Acc. Chem. Res. 49 (2016) 1389.

[12] Y. Dang, X. Deng, J. Guo, C. Song, W. Hu, Z.-X. Wang, J. Am. Chem. Soc. 138 (2016) 2712.

[13] T. Gensch, M.N. Hopkinson, F. Glorius, J. Wencel-Delord, Chem. Soc. Rev. 45 (2016) 2900.

[14] H. Tang, X.-R. Huang, J. Yao, H. Chen, J. Org. Chem. 80 (2015) 4672.

[15] J.F. Hartwig, J. Am. Chem. Soc. 138 (2015) 2.

[16] J. Wencel-Delord, T. Dröge, F. Liu, F. Glorius, Chem. Soc. Rev. 40 (2011) 4740.

[17] T.W. Lyons, M.S. Sanford, Chem. Rev. 110 (2010) 1147.

[18] K. Yamamoto, K. Higuchi, S. Kuwata, Y. Hayashi, S. Kawauchi, T. Takata, Dalton Trans. 49 (2020) 2781.

[19] R. Deka, A. Sarkar, R.J. Butcher, P.C. Junk, D.R. Turner, G.B. Deacon, H.B. Singh, Organometallics 39 (2020) 334.

[20] D.E. Janzen, M.A. Bruening, A.A. Mamiya, L.E. Driscoll, D.A. da Silva Filho, Dalton Trans. 48 (2019) 11520.

[21] Q.-L. Yang, C.-Z. Li, L.-W. Zhang, Y.-Y. Li, X. Tong, X.-Y. Wu, T.-S. Mei, Organometallics 38 (2019) 1208.

[22] Y.B. Dudkina, K.V. Kholin, T.V. Gryaznova, D.R. Islamov, O.N. Kataeva, I.Kh. Rizvanov, A.I. Levitskaya, O.D. Fominykh, M.Yu. Balakina, O.G. Sinyashina, Y.H. Budnikova, Dalton Trans. 46 (2017) 165.

[23] P. Kar, M. Yoshida, A. Kobayashi, L. Routaboul, P. Braunstein, M. Kato, Dalton Trans. 45 (2016) 14080.

[24] B.N. Nguyen, L.A. Adrio, T. Albrecht, A.J.P. White, M.A. Newton, M. Nachtegaal, S.J.A. Figueroa, K.K.M. Hii, Dalton Trans. 44 (2015) 16586.

[25] J.M. Racowski, A.R. Dick, M.S. Sanford, J. Am. Chem. Soc. 131 (2009) 10974.

[26] G.L. Edwards, D.St.C. Black, G.B. Deacon, L.P.G. Wakelin, Can. J. Chem. 83 (2005) 980.

[27] P. Jolliet, M. Gianini, A. von Zelewsky, G. Bernardinelli, H. Stoeckli-Evans, Inorg. Chem. 35 (1996) 4883.

[28] X.-Q. Zhou, A. Busemann, M.S. Meijer, M.A. Siegler, S. Bonnet, Chem. Commun. 55 (2019) 4695.

[29] J. Lin, C. Zou, X. Zhang, Q. Gao, S. Suo, Q. Zhuo, X. Chang, M. Xie, W. Lu, Dalton Trans. 48 (2019) 10417.

[30] Q. Wan, W.-P. To, C. Yang, C.-M. Che, Angew. Chem., Int. Ed. 57 (2018) 3089.

[31] C. Zou, J. Lin, S. Suo, M. Xie, X. Chang, W. Lu, Chem. Commun. 54 (2018) 5319.

[32] M. Zvirzdinaite, S. Garbe, N. Arefyeva, M. Krause, R. von der Stück, A. Klein, Eur. J. Inorg. Chem. (2017) 2011.

[33] T.T.-H. Fong, C.-N. Lok, C.Y.-S. Chung, Y.-M. E. Fung, P.-K. Chow, P.-K. Wan, C.-M. Che, Angew. Chem., Int. Ed. 55 (2016) 11935.

[34] A. Zucca, G.L. Petretto, M.L. Cabras, S. Stoccoro, M.A. Cinellu, M. Manassero, G. Minghetti, J. Organomet. Chem. 694 (2009) 3753.
[35] F. Neve, A. Crispini, C. Di Pietro, S. Campagna, Organometallics 21 (2002) 3511.
[36] S.-W. Lai, T.-C. Cheung, M.C.W. Chan, K.-K. Cheung, S.-M. Peng, C.-M. Che, Inorg. Chem. 39 (2000) 255.
[37] A. Zucca, M.A. Cinellu, M.V. Pinna, S. Stoccoro, G. Minghetti, M. Manassero, M. Sansoni, Organometallics 19 (2000) 4295.
[38] T. Karlen, A. Ludi, H.-U. Güdel, H. Riesen, Inorg. Chem. 30 (1991) 2250.
[39] E.C. Constable, R.P.G. Henney, T.A. Leese, D.A. Tocher, J. Chem. Soc., Dalton Trans. (1990) 443.
[40] E.C. Constable, R.P.G. Henney, T.A. Leese, D.A. Tocher, J. Chem. Soc., Chem. Commun. (1990) 513.
[41] J. Föller, D.H. Friese, S. Riese, J.M. Kaminski, S. Metz, D. Schmidt, F. Würthner, C. Lambert, C.M. Marian, Phys. Chem. Chem. Phys. 22 (2020) 3217.
[42] L. Liu, X. Wang, F. Hussain, C. Zeng, B. Wang, Z. Li, I. Kozin, S. Wang, ACS Appl. Mater. Interfaces 11 (2019) 12666.
[43] Y. Yao, C.-L. Hou, Z.-S. Yang, G. Ran, L. Kang, C. Li, W. Zhang, J. Zhang, J.-L. Zhang, Chem. Sci. 10 (2019) 10170.
[44] P.-K. Chow, G. Cheng, G.S.M. Tong, C. Ma, W.-M. Kwok, W.-H. Ang, C.Y.-S. Chung, C. Yang, F. Wang, C.-M. Che, Chem. Sci. 7 (2016) 6083.
[45] P.-K. Chow, W.-P. To, K.-H. Low, C.-M. Che, Chem. -Asian J. 9 (2014) 534.
[46] P.K. Chow, C. Ma, W.-P. To, G.S.M. Tong, S.-L. Lai, S.C.F. Kui, W.-M. Kwok, C.-M. Che, Angew. Chem., Int. Ed. 52 (2013) 11775.
[47] B. Soro, S. Stoccoro, G. Minghetti, A. Zucca, M.A. Cinellu, S. Gladiali, M. Manassero, M. Sansoni, Organometallics 24 (2005) 53.
[48] R.H. Fath, S.J. Hoseini, J. Organomet. Chem. 828 (2017) 16.
[49] P. Ramírez-López, A. Ros, A. Romero-Arenas, J. Iglesias-Sigüenza, R. Fernández, J.M. Lassaletta, J. Am. Chem. Soc. 138 (2016) 12053.
[50] H. Baier, A. Kelling, U. Schilde, H.-J. Holdt, Z. Anorg. Allg. Chem. 642 (2016) 140.
[51] C. Icsel, V.T. Yilmaz, Y. Kaya, H. Samli, W.T.A. Harrison, O. Buyukgungord, Dalton Trans. 44 (2015) 6880.
[52] A. Zucca, G.L. Petretto, S. Stoccoro, M.A. Cinellu, G. Minghetti, M. Manassero, C. Manassero, L. Male, A. Albinati, Organometallics 25 (2006) 2253.
[53] A. Zucca, M.A. Cinellu, G. Minghetti, S. Stoccoro, M. Manassero, Eur. J. Inorg. Chem. (2004) 4484.
[54] A. Hofmann, L. Dahlenburg, R. van Eldik, Inorg. Chem. 42 (2003) 6528.
[55] A. Zucca, A. Doppiu, M.A. Cinellu, S. Stoccoro, G. Minghetti, M. Manassero, Organometallics 21 (2002) 783.
[56] A. Klein, B. Rausch, A. Kaiser, N. Vogt, A. Krest, J. Organomet. Chem. 774 (2014) 86.
[57] A. Klein, A. Sandleben, N. Vogt, Proc. Nat. Acad. Sci. India (PNASI) Section-A; Phys. Sci. 86 (2016) 533.
[58] A. Sandleben, N. Vogt, G. Hörner, A. Klein, Organometallics 37 (2018) 3332.
[59] N. Vogt, V. Sivchik, A. Sandleben, G. Hörner, A. Klein, Molecules 25 (2020) 997.
[60] C.M. Anderson, N. Oh, T.A. Balema, F. Mastrocinque, C. Mastrocinque, D. Santos, M.W. Greenberg, J.M. Tanski, Tetrahedron Lett. 57 (2016) 4574.
[61] I. Omae, J. Organomet. Chem. 696 (2011) 1128.
[62] A.G. Algarra, S.A. Macgregor, J.A. Panetier, Mechanistic Studies of C-X Bond Activation at Transition-Metal Centers in J. Reedijk, K. Poeppelmeier (Eds.), Comprehensive Inorganic Chemistry II (Second Edition), Publisher: Elsevier, Amsterdam, 2013, pp. 635-694.
[63] P. Vermeeren, X. Sun, F.M. Bickelhaupt, Sci. Rep. 8 (2018) 10729.
[64] A. Diefenbach, G.T. de Jong, F.M. Bickelhaupt, J. Chem. Theory Comput. 1 (2005) 286.
[65] P.-L.T. Boudreault, M.A. Esteruelas, E. Mora, E. Oñate, J.-Y. Tsai, Organometallics 37 (2018) 3770.
[66] H. Wu, M.B. Hall, J. Phys. Chem. A 113 (2009) 11706.
[67] C.M. Anderson, M.W. Greenberg, T.A. Balema, L.M. Duman, N. Oh, A. Hashmi, L. Ladner, K. Jain, D. Yu, J.M. Tanski, Tetrahedron Lett. 56 (2015)

6352.
[68] C.M. Anderson, G. Brown, M.W. Greenberg, D. Yu, N. Bowen, R. Ahmed, M. Yost-Bido, A. Wray, Tetrahedron Lett. 60 (2019) 151.
[69] M. Crespo, M. Martínez, S.M. Nabavizadeh, M. Rashidi, Coord. Chem. Rev. 279 (2014) 115.
[70] A. Klein, M. Niemeyer, Z. Anorg. Allgem. Chem. 626 (2000) 1191.
[71] K. Butsch, R. Gust, A. Klein, I. Ott, M. Romanski, Dalton Trans. 39 (2010) 4331.
[72] A. Klein, R. Lepski, Z. Anorg. Allg. Chem. 635 (2009) 878.
[73] A. Klein, Z. Anorg. Allgem. Chem. 627 (2001) 645.
[74] A. Klein, W. Kaim, Organometallics 14 (1995) 1176.
[75] A. Haseloer, R. Jordan, L.M. Denkler, M. Reimer, S. Olthof, I. Schmidt, K. Meerholz, G. Hörner, A. Klein, Dalton Trans. 50 (2021) 4311.
[76] J.C. Fuggle, N. Martensson, J. Electron Spectr. Relat. Phenom. 21 (1980) 275.
[77] N. Vogt, A. Sandleben, L. Kletsch, S. Schäfer, M.T. Chin, D.A. Vicic, G. Hörner, A. Klein, Organometallics 40 (2021) 1776.
[78] L.E. Roy, P.J. Hay, R.L. Martin, J. Chem. Theory Comput. 4 (2008) 1029.
[79] A. Klein, A. Kaiser, B. Sarkar, M. Wanner, J. Fiedler, Eur. J. Inorg. Chem. (2007) 965.
[80] W. Kaim, J. Fiedler, Chem. Soc. Rev. 38 (2009) 3373.
[81] M. Krejčík, M. Daňek, F. Hartl, J. Electroanal. Chem. 317 (1991) 179.
[82] G.M. Sheldrick, Acta Crystallogr. Sect. A Found. Crystallogr. 71 (2015) 3.
[83] G.M. Sheldrick, SHELXL-2017/1, Program for the Solution of Crystal Structures; University of Göttingen: Göttingen, Germany, 2017.
[84] G.M. Sheldrick, Crystal structure refinement with SHELXL. Acta Crystallogr. Sect. C Struct. Chem. 71 (2015) 3.
[85] STOE X-RED. Data Reduction Program, Version 1.31/Windows; STOE & Cie: Darmstadt, Germany (2005).
[86] STOE X-SHAPE. Crystal Optimisation for Numerical Absorption Correction, Version 1.06/Windows; STOE & Cie: Darmstadt, Germany (1999).
[87] J.W. Mintmire, B.I. Dunlap, Phys. Rev. A 25 (1982) 88.
[88] C.K. Skylaris, L. Gagliardi, N.C. Handy, A.G. Ioannou, S. Spencer, A. Willetts, J. Mol. Struct.: THEOCHEM 501-50 (2000) 229.
[89] TURBOMOLE Program Package for ab initio Electronic Structure Calculations V7.5, Turbomole GmbH, Karlsruhe, Germany, 2020.
[90] C. Steffen, K. Thomas, U. Huniar, A. Hellweg, O. Rubner, A. Schroer, J. Comput. Chem. 31 (2010) 2967.
[91] A. Schäfer, H. Horn, R. Ahlrichs, J. Chem. Phys. 97 (1992) 2571.
[92] A. Schäfer, C. Huber, R. Ahlrichs, J. Chem. Phys. 100 (1994) 5829.
[93] A. Klamt, J. Phys. Chem. 99 (1995) 2224.
[94] A. Klamt, V. Jonas, T. Bürger, J.C.W. Lohrenz, J. Phys. Chem. A 102 (1998) 5074.
[95] D.R. Lide (Ed.), CRC Handbook of Chemistry and Physics, 87th Edition, Taylor & Francis, 2006.
[96] C. Lee, W. Yang, R.G. Parr, Phys. Rev. B 37 (1988) 785.
[97] A.D. Becke, J. Chem. Phys. 98 (1993) 5648.
[98] A.D. Becke, J. Chem. Phys. 98 (1993) 1372.
[99] P.J. Hay, W.R. Wadt, J. Chem. Phys. 82 (1985) 299.
[100] P.J. Hay, W.R. Wadt, J. Phys. Chem. 82 (1985) 270.